

Role of Interfacial Charge Transfer State in Charge Generation and Recombination in Low-Bandgap Polymer Solar Cell

Shunsuke Yamamoto,[†] Hideo Ohkita,^{,†,‡} Hiroaki Benten,[†] and Shinzaburo Ito[†]*

[†]Department of Polymer Chemistry, Graduate School of Engineering, Kyoto University, Katsura,
Nishikyo, Kyoto 615-8510, Japan.

[‡]Japan Science and Technology Agency (JST), PRESTO, 4-1-8 Honcho Kawaguchi, Saitama 332-0012,
Japan.

KEYWORDS Conjugated Polymer, Fullerene, Organic Solar Cells, Transient Absorption Spectroscopy

ABSTRACT

The charge carrier dynamics in blend films of poly[2,6-(4,4-bis-(2-ethylhexyl)-4*H*-cyclopenta[2,1-*b*;3,4-*b'*]dithiophene)-*alt*-4,7-(2,1,3-benzothiadiazole)] (PCPDTBT) and [6,6]-phenyl-C₆₁-butyric acid methyl ester (PCBM) was studied by transient absorption spectroscopy in order to address the origin of limited external quantum efficiency (EQE) of this solar cell compared to that of a benchmark solar cell composed of regioregular poly(3-hexylthiophene) (RR-P3HT) and PCBM. Upon photoexcitation, PCPDTBT singlet excitons promptly convert to the interfacial charge transfer (CT) state that is a coulombically bound charge pair of PCPDTBT polaron and PCBM anion at the heterojunction with almost 100% efficiency in a picosecond. In other words, the exciton diffusion efficiency η_{ED} and charge transfer efficiency η_{CT} are 100% in this blend, which are higher than and comparable to those of the RR-P3HT/PCBM solar cell, respectively. On a time scale of nanoseconds, 70% of the PCPDTBT bound polarons are dissociated into free charge carriers and the others recombine geminately to the ground state through the CT state. The charge dissociation efficiency $\eta_{CD} = 70\%$ is lower than that of RR-P3HT/PCBM solar cells. The PCPDTBT dissociated polarons recombine bimolecularly on a time scale of nano- to microseconds with a charge lifetime of $\sim 10^{-7}$ s, which is shorter than that observed for RR-P3HT/PCBM blends. In summary, the lower charge dissociation efficiency and shorter charge lifetime are the limiting factors for the photovoltaic performance of PCPDTBT/PCBM solar cells. Furthermore, the origin of such limitation is also discussed in terms of the charge dissociation and recombination through the interfacial CT state in PCPDTBT/PCBM blends.

1. Introduction

---<<< Figure 1 >>>---

Currently, the power conversion efficiency (PCE) of polymer/fullerene solar cells is approaching 10%.^{1,2} One of the key materials to the remarkable progress is low-bandgap polymers, which can absorb more photons in the near-IR region than conventional conjugated polymers such as regioregular poly(3-hexylthiophene) (RR-P3HT) and therefore can increase the short-circuit current density (J_{SC}) effectively. Most of the low-bandgap polymers have electron donor and acceptor units arranged alternatively in the main chain.³⁻⁵ The donor/acceptor linkage induces an intramolecular donor-acceptor interaction resulting in the reduction of the bandgap energy. Poly[2,6-(4,4-bis-(2-ethylhexyl)-4*H*-cyclopenta[2,1-b;3,4-b']dithiophene)-*alt*-4,7-(2,1,3-benzothiadiazole)] (PCPDTBT) is a typical low-bandgap polymer that consists of cyclopentadithiophene donor units and the benzothiadiazole acceptor units in the main chain (**Figure 1a**). Because of the donor-acceptor interaction, this polymer has a red-shifted absorption up to ~800 nm. The PCPDTBT-based polymer solar cell was first reported in 2006,⁶ and its PCE was improved in excess of 5% by using an additive with a high boiling point.⁷ In particular, J_{SC} exceeds 15 mA cm^{-2} , which cannot be obtained by conventional polymers studied so far. However, this is still far below the maximum J_{SC} of 23.8 mA cm^{-2} for the 100% light harvesting up to 800 nm.⁴ This is because the external quantum efficiency (EQE) is as low as 50% for the PCPDTBT-based polymer solar cell.⁶⁻¹⁰ In other words, the potential PCE would exceed 8% if EQE could be improved up to 80% as is the case for a benchmark solar cell composed of RR-P3HT and [6,6]-phenyl- C_{61} -butyric acid methyl ester (PCBM). Previous studies have shown the rapid charge generation (<0.1 ps) by ultrafast transient absorption spectroscopy of PCPDTBT/PCBM blends.^{11,12} On the other hand, device analysis studies have shown that the bimolecular recombination controls the solar cell performance of the PCPDTBT/PCBM solar cell.^{8,13-15} However, the origin of the low EQE is still not fully understood:

the charge dissociation efficiency is not evaluated quantitatively or little is known about the mechanism of the bimolecular recombination.

Herein we comprehensively study the charge generation and recombination dynamics in PCPDTBT/PCBM blends by transient absorption spectroscopy. Consequently, we found that singlet excitons convert to the interfacial charge transfer (CT) state that is a bound charge pair of PCPDTBT polaron and PCBM anion at the heterojunction with 100% efficiency followed by the charge dissociation into free charge carriers with 70% efficiency in competition with the geminate recombination with 30% efficiency. Considering the delocalization of singlet excitons, we found a good correlation between the singlet exciton size and the charge dissociation efficiency: larger singlet excitons provide higher charge dissociation efficiency. Furthermore, we demonstrated that the fast bimolecular recombination is due to the rapid recombination via the CT state by comparing the slow recombination in RR-P3HT/PCBM blends. Comparing with RR-P3HT/PCBM solar cells, we discuss the origin of the limited EQE of PCPDTBT/PCBM solar cells in terms of the charge generation and recombination mechanism.

2. Experimental

Materials: The following chemicals were used without further purification: PCBM (99.9%, Frontier Carbon), 1,8-diiodooctane (DIO, Wako), and chlorobenzene (Wako). The low-bandgap polymer PCPDTBT was synthesized as described elsewhere.¹⁶

Sample Fabrication: Polymer/fullerene blend films were prepared on glass substrates by spin-coating from a chlorobenzene solution of PCPDTBT and PCBM with 2 vol% of DIO at a spin rate of 1000 rpm after the spin rate of 400 rpm (10 s) under ambient conditions. The film thickness was typically 300 nm. The weight fraction of PCBM was set at 50 wt%. The blend solution was stirred at 40 °C overnight to be dissolved homogeneously. Before the spin-coating, the glass substrates were cleaned by ultrasonic treatment in toluene, acetone, and ethanol sequentially for 15 min each, and then with a UV–ozone

cleaner (Nippon Laser & Electronics Lab., UV253) for 1 h.

Measurements: Transient absorption data were collected in a nitrogen-purged quartz cuvette with three different spectrometers as described below. The femtosecond transient absorption data were collected with a pump and probe transient absorption spectroscopy system (Ultrafast Systems, Helios). The pump light was fundamental pulses (800 nm, fwhm 100 fs, 1 kHz) from a regeneratively amplified Ti-sapphire laser (Spectra-Physics, Hurricane). The probe beam was detected with a CMOS linear sensor (Ultrafast Systems, SPEC-VIS) for the visible wavelength range from 400 to 900 nm and with an InGaAs linear diode array sensor (Ultrafast Systems, SPEC-NIR) for the near-IR wavelength range from 850 to 1600 nm. The typical noise level of this system is lower than 2×10^{-4} in absorbance. The nanosecond transient absorption data were collected with a pump and probe transient absorption spectroscopy system (Ultrafast Systems, EOS). The excitation source was the same as that employed in the femtosecond system. The continuum probe pulse (380 to 1700 nm, 0.5 ns pulse width, 20 kHz repetition rate) was generated by focusing a Nd:YAG laser pulse into a photonic crystal fiber. The probe pulses were synchronized with the femtosecond amplifier, and the delay time was controlled by a digital delay generator electrically (CNT-90, Pendulum Instruments). For the microsecond transient absorption measurement, the sample was excited with a light pulse (800 nm, 4 Hz) from a dye laser (Photon Technology International, GL-301) that was pumped with a nitrogen laser (Photon Technology International, GL-3300), and probed with a monochromatic light from a 50-W quartz tungsten halogen lamp (Thermo–ORIEL, Model 66997) with a light intensity controller (Thermo–ORIEL, Model 66950), which was equipped with appropriate optical cut-filters and two monochromators (Ritsu, MC-10N) before and after the sample to reduce stray light, scattered light, and emission from the sample. The probe light was detected with a pre-amplified Si photodiode (Costronics Electronics) for the visible wavelength range from 700 to 1100 nm, and pre-amplified InGaAs photodiode (Newport 1811s) for the near-infrared wavelength range from 900 to 1500 nm. The detected signal was sent to the main amplification system with an electronic band-pass filter (Costronics Electronics) to improve the signal-

to-noise ratio. The amplified signal was collected with a 200-MHz digital oscilloscope (Tektronix, TDS2022), which was synchronized with a trigger signal of the laser pulse from a photodiode (Thorlabs, DET10A). The detectable absorbance change ΔOD is as small as $\sim 10^{-5} - 10^{-6}$ depending on the measuring time domain.

3. Results

Figure 1c shows the absorption spectra of PCPDTBT/PCBM (50:50 w/w) blend films fabricated with DIO as an additive. Note that all the blend films employed in this study were fabricated with DIO unless otherwise noted. A large absorption band observed at around 700 nm is ascribed to the intramolecular donor–acceptor interaction band as reported previously.⁶ In addition, an absorption shoulder observed at around 800 nm is ascribed to the ordering of PCPDTBT as reported previously.^{17,18} Comparing to the absorption of PCPDTBT in toluene, it is found that the ordered PCPDTBT domains can be selectively excited at 800 nm. On the other hand, no fluorescence was observed for the blend films. In other words, the exciton quenching efficiency is almost 100% for PCPDTBT/PCBM blend films. Furthermore, the hole mobility in the blend was evaluated to be $\mu_{\text{th}} = 4 \times 10^{-4} \text{ cm}^2 \text{ V}^{-1} \text{ s}^{-1}$ (see the Supporting Information).

---<<< Figure 2 >>>---

Figure 2a shows the transient absorption spectra of PCPDTBT neat films immediately after the laser excitation (<0.1 ps) at 800 nm under various excitation intensities. At low excitation intensities, the absorption peak was found at around 1500 nm. This absorption band is ascribed to PCPDTBT singlet excitons because the decay constant is consistent with the fluorescence lifetime (220 ps). At high excitation intensities, an additional absorption shoulder was observed at around 1200–1300 nm. This absorption is ascribed to PCPDTBT polarons as described below. Figure 2b shows the initial

absorbance of PCPDTBT singlet excitons and polarons under various excitation intensities. Below a fluence of $16 \mu\text{J cm}^{-2}$, the slope for the initial absorbance of PCPDTBT singlet exciton was unity, suggesting that bimolecular processes are negligible. Above the fluence of $16 \mu\text{J cm}^{-2}$, the slope was 0.5, suggesting bimolecular quenching of PCPDTBT singlet exciton. On the other hand, above the fluence of $16 \mu\text{J cm}^{-2}$ the slope for the initial absorbance of PCPDTBT polaron was 2, suggesting that polarons are generated via a bimolecular reaction. Thus, we conclude that PCPDTBT polarons are generated within a laser pulse width of 0.1 ps via the singlet–singlet exciton annihilation without exciton diffusion (or two-photon absorption). From the photon density at the threshold ($= 1.6 \times 10^{18} \text{ cm}^{-3}$), the interaction radius of the PCPDTBT singlet exciton is estimated to be $r_{\text{ex}} = 4.2 \text{ nm}$ at $<0.1 \text{ ps}$ after the excitation at 800 nm as reported previously.¹⁹ Note that the singlet exciton is simply assumed to be a sphere.

---<<< Figure 3 >>>---

Figure 3 shows the transient absorption spectra of a PCPDTBT/PCBM blend film from $<0.1 \text{ ps}$ to 3 ns after the laser excitation at 800 nm. As mentioned before, the ordered PCPDTBT domains are selectively excited at this wavelength and no PCBM is excited. Thus, we can focus on the charge generation dynamics from PCPDTBT singlet exciton in the ordered domains. As shown in Figure 3, a broad absorption up to 1500 nm was observed immediately after the laser excitation, the absorption at around 1500 nm disappeared rapidly, and instead the absorption band at around 1250 nm was pronounced in a few picoseconds. The absorption band at around 1250 nm subsequently decayed in a few nanoseconds. Note that the transient spectra are dependent on the excitation intensity and wavelength: prompt exciton decay and charge generation due to the singlet–singlet exciton annihilation are involved under higher excitation intensities, and PCPDTBT polaron formation in disordered domains is involved upon the photoexcitation at short wavelengths (see the Supporting Information).

The absorption band at 1500 nm is ascribed to PCPDTBT singlet excitons as mentioned above. On the other hand, the absorption band at 1250 nm is ascribed to PCPDTBT polarons^{20,21} because it was still observed on a time scale of microseconds and was not quenched in an oxygen atmosphere (see the Supporting Information). Note that PCBM anion has a small absorption band with a molar absorption coefficient of $6000 \text{ M}^{-1} \text{ cm}^{-1}$ at 1020 nm, which is much smaller than that of PCPDTBT polarons.²² In summary, PCPDTBT singlet excitons rapidly disappear and instead PCPDTBT polarons are rapidly generated in a few picoseconds. This is consistent with the efficient fluorescence quenching.

---<<< Figure 4 >>>---

To analyze the charge generation dynamics in detail, we resolved the transient absorption spectra into PCPDTBT singlet exciton and polaron by spectral simulation as shown in **Figure 4a**. The absorption spectrum of the PCPDTBT neat film at <0.1 ps can be used as that of PCPDTBT singlet excitons. The absorption spectrum at 2 ps of the PCPDTBT/PCBM blend film can be used as that of PCPDTBT polarons because the spectral change is finished before 2 ps. As a result, we obtained the time evolution of PCPDTBT singlet excitons and polarons generated in PCPDTBT/PCBM blend films excited at 800 nm. As shown in Figure 4b, PCPDTBT singlet excitons decayed and PCPDTBT polarons were generated with the same time constant. This suggests that PCPDTBT polarons are directly generated from PCPDTBT singlet excitons. The charge generation time constant is evaluated to be 0.6 ps for the PCPDTBT/PCBM blend. Furthermore, 35% of PCPDTBT polarons were promptly generated within the laser pulse width (~ 0.1 ps).

---<<< Figure 5 >>>---

Figure 5 shows the transient decay of PCPDTBT polaron monitored at 1240 nm in the sub-nanosecond time regime after the laser excitation at 800 nm under various excitation conditions. The decay dynamics is independent of the excitation intensity under the low excitation condition ($<20 \mu\text{J cm}^{-2}$), suggesting monomolecular recombination. Furthermore, the photobleaching at 700 nm recovered with the same time constant (see the Supporting Information). Therefore, the decay dynamics is ascribed to the monomolecular recombination of PCPDTBT bound polarons to the ground state. Indeed, the decay dynamics can be well fitted by a single exponential function with a constant fraction: $\Delta\text{OD} = A \exp(-t/\tau_m) + B$. From the fitting, the decay constant and each fraction are evaluated to be $\tau_m = 480 \text{ ps}$ and $A : B = 30 : 70$, respectively. Note that the decay dynamics is dependent on the excitation intensity under the high excitation condition ($>20 \mu\text{J cm}^{-2}$), suggesting bimolecular recombination of dissociated polarons which are promptly generated by the singlet–singlet exciton annihilation as mentioned before. Such rapid bimolecular recombination has been reported in a recent paper.²³

---<<< Figure 6 >>>---

Figure 6a shows the transient decay of PCPDTBT polaron monitored at 1240 nm from 1 ns to 1 ms after the laser excitation at 800 nm under various excitation conditions. The charge carrier density was estimated as described in the Supporting Information. Note that the transient signals were not quenched by oxygen atmosphere, suggesting that no triplet exciton is involved in the transient signals. For comparison, the transient decay of P3HT polaron monitored at 1000 nm in RR-P3HT/PCBM is also shown in Figure 6b. No decay was observed at an early time stage, and the power-law decay was observed at a later time stage. All the decay dynamics can be well fitted by an empirical power-law equation

$$n(t) = n_0(1 + at)^{-\alpha} \quad (1)$$

where $n(t)$ is the carrier density at a delay time t , n_0 is the carrier density at $t = 0$, and α and a are

parameters. The exponent α represents the slope of the decay in the log–log plots. The inverse of the parameter a is indicative of the time for the carrier density to start decreasing. As shown in the figure, the exponent is constant $\alpha = 0.5$ for PCPDTBT/PCBM and RR-P3HT/PCBM, which are in agreement with previous reports.^{20,24} The power-law kinetics with $\alpha < 1$ is characteristic of trap-limited bimolecular recombination.²⁵ The exponent α of PCPDTBT/PCBM and RR-P3HT/PCBM is independent of the excitation intensity. On the other hand, the parameter a of PCPDTBT/PCBM is almost independent of the excitation intensity while the parameter a of RR-P3HT/PCBM decreases with increasing excitation intensity. The charge lifetime will be discussed later on the basis of parameter a .

4. Discussion

First, we focus on the charge generation dynamics in PCPDTBT/PCBM blends. As mentioned before, PCPDTBT bound polarons are rapidly generated with a time constant of 0.6 ps. This is much faster than that observed for RR-P3HT/PCBM crystalline blends (8 ps), but similar to that observed for RRa-P3HT/PCBM amorphous blends (0.2 ps).²⁶ This finding suggests that PCBM molecules are likely to be molecularly dispersed and hence efficiently quench neighboring PCPDTBT singlet excitons even though the DIO additive can effectively promote the ordering of PCPDTBT and the phase separation in PCPDTBT/PCBM blends as reported previously.^{27,28} Indeed, we found larger phase separation for PCPDTBT/PCBM blend films fabricated with DIO.¹⁶ We therefore conclude that large phase-separated domains in PCPDTBT/PCBM blends are not pure but should involve minor counterpart. This is consistent with a recent study, which has shown multi-length-scale morphologies in PCPDTBT/PCBM blends.²⁹ Here we note that the charge generation is much more rapid than the lifetime of the singlet exciton. In other words, the exciton diffusion efficiency η_{ED} to and the charge transfer efficiency η_{CT} at a donor/acceptor interface are estimated to be 100% in PCPDTBT/PCBM blend films. The almost 100% charge generation yield is the same as those for amorphous blends such as RRa-P3HT and PCBM²⁶ or a carbazole-based copolymer (PCDTBT) and PCBM,³⁰ but larger than those for RR-

P3HT/PCBM crystalline blends.

Next, we move on to the monomolecular recombination dynamics on a time scale of sub-nanoseconds. Before discussing the decay dynamics, we should note that there is no spectral difference between PCPDTBT dissociated polaron and PCPDTBT bound polaron at the interface (the interfacial CT state). In contrast, as reported previously,²⁴ P3HT polarons generated in RR-P3HT/PCBM blend films exhibit different absorption bands: P3HT delocalized polarons in crystalline domains (700 nm), P3HT localized polarons in disordered domains (1000 nm), and P3HT polarons bound to PCBM anions in disordered domains (800 nm). This is probably because PCPDTBT forms amorphous films unlike crystalline RR-P3HT.^{18,31,32} Here we therefore assign the transient absorption on the basis of the decay analysis instead of the spectral analysis. As mentioned before, the monomolecular decay dynamics of PCPDTBT polaron is in good agreement with the recovery dynamics of the photobleaching, suggesting the geminate recombination to the ground state. Furthermore, this decay constant $\tau_m = 480$ ps is in good agreement with the lifetime of the interfacial CT state emission at 1100 nm observed for PCPDTBT/PCBM blend films (480 ps).³³ We therefore conclude that the PCPDTBT polarons initially form interfacial CT state. Here, we define the interfacial CT state as a coulombically bound charge pair of PCPDTBT polaron and PCBM radical anion. Subsequently, the interfacial CT states are dissociated into dissociated charge carriers or recombine to the ground state with a time constant of 480 ps. In other words, the monomolecular recombination is ascribed to the geminate recombination from the interfacial CT state to the ground state. From the fitting parameters, the charge dissociation efficiency η_{CD} is estimated to be 70%, which is consistent with a recent paper.³⁴ We note that η_{CD} is much larger than the prompt polaron generation yield at <0.1 ps (35%) as mentioned above. If the dissociated charges were due to the prompt polaron generation at <0.1 ps as proposed in the recent paper,³⁴ η_{CD} would be the same as the prompt polaron generation yield. However, this is not the case. We therefore conclude that the interfacial CT state is an intermediate source of the charge dissociation. Thus, the charge dissociation and recombination rates are estimated to be $k_{dis} = 1 \times 10^9$ s⁻¹ and $k_{rec} = 6 \times 10^8$ s⁻¹,

respectively. This charge dissociation efficiency ($\eta_{CD} = 70\%$) is larger than that for RRa-P3HT/PCBM (31%) but lower than that for P3HT/PCBM blend films (80–90%). On the other hand, the interaction radius of the PCPDTBT singlet exciton is $r_{ex} = 4.2$ nm, which is larger than that of the RRa-P3HT singlet exciton ($r_{ex} = 3.2$ nm) and smaller than that of the RR-P3HT singlet exciton ($r_{ex} = 4.3\text{--}6.7$ nm).^{19,35,36} In other words, singlet excitons of PCPDTBT are more delocalized than that of RRa-P3HT, but more localized than that of RR-P3HT. Interestingly, there is a good correlation between η_{CD} and the interaction radius of singlet excitons, as we previously proposed.^{19,26} More delocalized singlet excitons would convert to electron–hole pairs with a larger separation distance at heterojunctions, and hence provide a larger η_{CD} . Durrant *et al.* pointed out that the effective Coulomb capture radius would be reduced to ~ 4 nm at a typical donor/fullerene heterojunction by considering the change in entropy associated with a change from a single exciton to two separated charges.³⁷ This is consistent with the correlation between η_{CD} and the interaction radius of singlet excitons. In a recent paper, Köhler *et al.* demonstrated that the more delocalized excited state gives the larger field-dependent photocurrent yield in planar heterojunctions.³⁸ We therefore conclude that the delocalization of singlet excitons has crucial impact on η_{CD} .

---<<< Figure 7 >>>---

---<<< Scheme 1 >>>---

Finally we discuss the bimolecular recombination dynamics on a timescale of nano- to microseconds. As described above, all the decay dynamics on this timescale can be well fitted by eq 1 with $\alpha = 0.5$, which is indicative of trap-limited bimolecular recombination. In the bimolecular charge recombination, the charge carrier density $n(t)$ is given by

$$\frac{dn(t)}{dt} = -\gamma(t)n^2(t) \quad (2)$$

where $\gamma(t)$ is the bimolecular recombination rate at a delay time t . By inserting eq 1 into eq 2, the time-dependent bimolecular recombination rate can be obtained by

$$\gamma(t) = \alpha \alpha n_0^{-1} (1 + \alpha t)^{(\alpha-1)} \quad (3)$$

Here, the charge carrier lifetime τ_c is defined by

$$\tau_c = [\gamma(0) n_0]^{-1} = (\alpha \alpha)^{-1} \quad (4)$$

As shown in **Figure 7**, the charge carrier lifetime τ_c is of the order of $\sim 10^{-7}$ s for PCPDTBT/PCBM blends, which is consistent with that estimated from the device analysis.⁸ On the other hand, the charge collection time at the short circuit can be roughly estimated to be $t_{CC}^{SC} = 2 \times 10^{-7}$ s as a transit time $d d_C / (V \mu)$ where d is the thickness of the active layer (100 nm), d_C is the average collection length ($= d/2$), V is the internal bias (0.6 V), and μ is the charge mobility ($4 \times 10^{-4} \text{ cm}^2 \text{ V}^{-1} \text{ s}^{-1}$). The charge collection time at the open circuit can be roughly estimated to be $t_{CC}^{OC} = 1 \times 10^{-6}$ s as a diffusion time $d_C^2 / (2D) = q d^2 / (8 k_B T \mu)$ where D is the diffusion constant of charge carriers ($= k_B T \mu / q$), k_B is the Boltzmann constant, T is temperature, and q is the elementary charge. Thus, the charge carrier lifetime τ_c in PCPDTBT/PCBM blends is comparable to t_{CC}^{SC} but shorter than t_{CC}^{OC} . This is different from that in RR-P3HT/PCBM blends where τ_c is as long as $\sim 10^{-5} - 10^{-4}$ s even under the open-circuit condition ($n \approx 10^{16} - 10^{17} \text{ cm}^{-3}$). Such a long lifetime of charge carriers is ascribed to the reduced bimolecular recombination in RR-P3HT/PCBM blends. As reported in many studies, the bimolecular recombination rate in RR-P3HT/PCBM blends is at least two orders of magnitude slower than the Langevin recombination rate γ_L .^{26,39,40} The reduced bimolecular recombination is indicative of the non-diffusion-limited recombination.⁴¹⁻⁴³ In the case of the non-diffusion-limited recombination, the recombination kinetics can be summarized as shown in **Scheme 1**. Under the steady state condition, the apparent recombination rate is given by $k_{rec} / (k_{rec} + k_{dis}) \gamma_L$ (see the Supporting Information).⁴⁴ As described above, k_{dis} is comparable to k_{rec} for PCPDTBT/PCBM blends. On the other hand, k_{dis} is much larger than k_{rec} for RR-P3HT/PCBM blends as reported previously.^{26,45,46} As a result, in contrast to RR-P3HT/PCBM blend films, the apparent recombination rate would be reduced only by a factor of $\sim 1/3$ compared to γ_L

for PCPDTBT/PCBM. Indeed, the bimolecular recombination rate in PCPDTBT/PCBM blends at $n \approx 10^{16} - 10^{17} \text{ cm}^{-3}$ is evaluated by eq 3 to be of the order of $\sim 10^{-10} \text{ cm}^3 \text{ s}^{-1}$, which is comparable to the Langevin recombination rate $\gamma_L = 8 \times 10^{-10} \text{ cm}^3 \text{ s}^{-1}$. We therefore conclude that the charge collection is one of the limiting factors to the device performance of PCPDTBT/PCBM solar cells because of the faster bimolecular recombination.

5. Conclusions

The charge generation and recombination dynamics in PCPDTBT/PCBM blend films were studied by transient absorption spectroscopy. In PCPDTBT neat films, only PCPDTBT singlet excitons are generated under low excitation conditions, but PCPDTBT polarons are additionally generated under high excitation conditions because of the singlet–singlet exciton annihilation. The interaction radius of the PCPDTBT singlet exciton is estimated to be $r_{\text{ex}} = 4.2 \text{ nm}$. In PCPDTBT/PCBM blend films, PCPDTBT singlet excitons promptly convert to the interfacial CT state that is a coulombically bound charge pair of PCPDTBT polaron and PCBM anion in a picosecond. In other words, the efficiency of the exciton diffusion to a donor/acceptor interface η_{ED} and the charge transfer at the interface η_{CT} is 100%. This is because PCBM molecules are likely to be homogeneously dispersed in amorphous blend films. Such 100% efficiency in η_{ED} and η_{CT} is found in other amorphous polymer blends such as RRa-P3HT/PCBM and PCDTBT/PCBM. On a time scale of nanoseconds, 70% of the interfacial CT state are dissociated into free charge carriers and the rest of them recombine geminately to the ground state. PCPDTBT/PCBM blend films have a dissociation efficiency η_{CD} is 70%, which is higher than that of RRa-P3HT/PCBM but lower than that of RR-P3HT/PCBM. Interestingly, there is a good correlation between the dissociation efficiency and the interaction radius of singlet excitons: $\eta_{\text{CD}} = 30\%$ and $r_{\text{ex}} = 3.2 \text{ nm}$ for RRa-P3HT, 70% and 4.2 nm for PCPDTBT, 80–90% and 4.3–6.7 nm for RR-P3HT. Thus, we conclude that the larger singlet exciton would provide a larger η_{CD} in polymer/PCBM blends. Subsequently, PCPDTBT dissociated polarons recombine bimolecularly with the power-law kinetics

from a time scale of tens nanoseconds, while P3HT polarons decay bimolecularly from a time scale of microseconds. Thus, the charge carrier lifetime in PCPDTBT/PCBM blends is estimated to be as short as $\sim 10^{-7}$ s, which is comparable to the charge collection time at the short circuit but shorter than the charge collection time at the open circuit. Such short lifetime of PCPDTBT dissociated polarons would lower the charge collection efficiency especially as the applied voltage is approaching V_{OC} . We therefore conclude that the limited EQE of PCPDTBT/PCBM solar cells is ascribed mainly to the lower charge dissociation and the shorter charge lifetime. In contrast, the long lifetime of P3HT dissociated polarons is due to the reduced bimolecular recombination. Such slow bimolecular recombination results from non-diffusion-limited recombination due to the high dissociation efficiency in P3HT/PCBM. In other words, the high dissociation efficiency would be the origin of the reduced bimolecular recombination in P3HT/PCBM. On the other hand, the faster recombination in PCPDTBT/PCBM results from the low dissociation efficiency, which is due to the formation of the interfacial CT state at the interface because the dissociation from the CT state is limited by the competitive geminate recombination. Such interfacial CT state would be formed from the smaller singlet exciton because of the larger Coulomb interaction. We therefore conclude that the larger singlet exciton is the key to the higher dissociation efficiency and the reduced recombination, which are essential for highly efficient polymer solar cells.

FIGURES

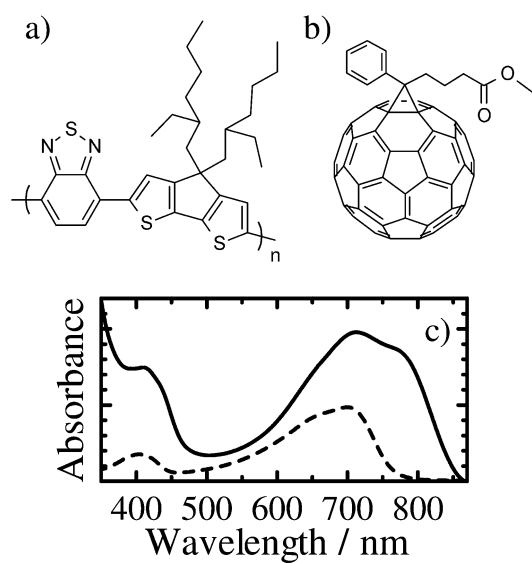


Figure 1. Chemical structures of materials employed in this study: a) PCPDTBT and b) PCBM. c) Absorption spectra of PCPDTBT/PCBM blend films (50:50 w/w) fabricated with DIO (solid line) and of toluene solution of PCPDTBT (broken line).

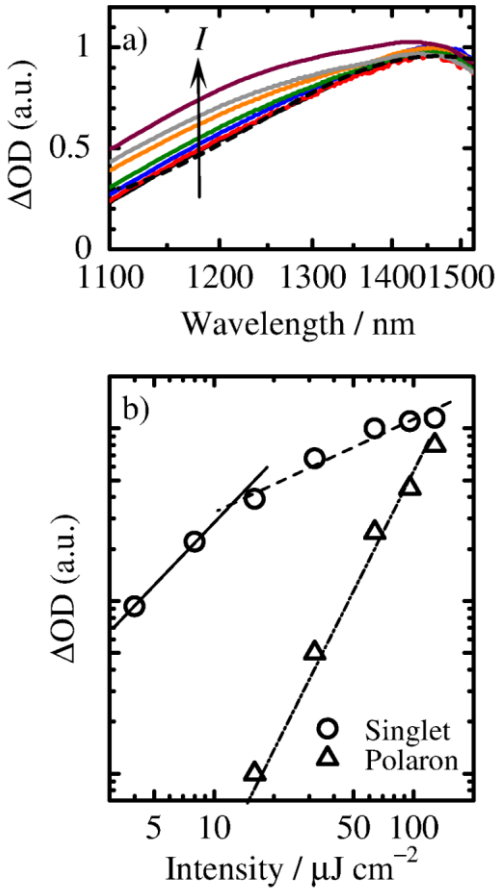


Figure 2. a) Transient absorption spectra of a PCPDTBT neat film immediately after the laser excitation (<0.1 ps) at 800 nm with fluences of 4 (black), 8 (red), 16 (blue), 32 (green), 64 (orange), 96 (gray), and $128 \mu\text{J cm}^{-2}$ (purple) from bottom to top in the panel. The broken line shows a fitting line by a Gaussian function for the spectrum at $4 \mu\text{J cm}^{-2}$. b) Log–log plots of the initial transient signals of a PCPDTBT neat film of PCPDTBT singlet (open circles) and PCPDTBT polaron (open triangles). The solid, broken, and dashed–dotted lines show the slope of 1, 0.5, and 2, respectively.

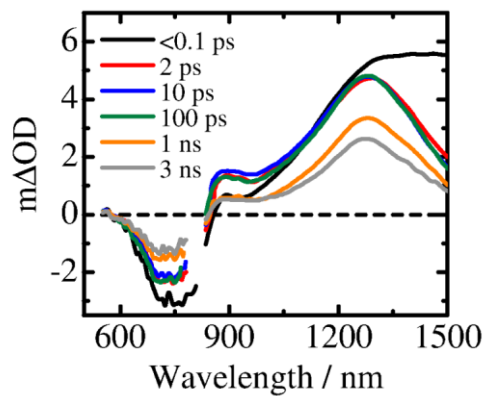


Figure 3. Transient absorption spectra of a PCPDTBT/PCBM blend film fabricated with DIO at <0.1 (black), 2 (red), 10 (blue), 100 (green), 1000 (orange), and 3000 ps (gray) after the laser excitation at 800 nm with a fluence of $4\ \mu\text{J cm}^{-2}$. The broken line shows the base line.

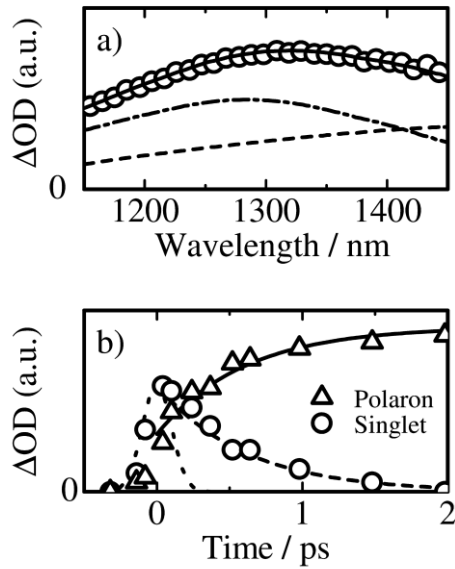


Figure 4. a) Transient absorption spectrum at 0.2 ps of the PCPDTBT/PCBM blend film fabricated with DIO (open circles). The solid line shows the spectrum simulated by the sum of the absorption spectra of PCPDTBT singlet exciton (broken line) and PCPDTBT polaron (dashed–dotted line). b) The time evolution of PCPDTBT singlet exciton (open circles) and PCPDTBT polaron (open triangles) in the PCPDTBT/PCBM blend film. The broken and solid lines show the fitting lines by exponential functions: $A \exp(-t/\tau_d)$ for the decay and $A[1 - \exp(-t/\tau_r)] + B$ for the rise kinetics with $\tau_d = \tau_r = 0.6$ ps and $A : B = 65 : 35$. The dotted line shows the instrument response function of the femtosecond transient absorption spectrometer.

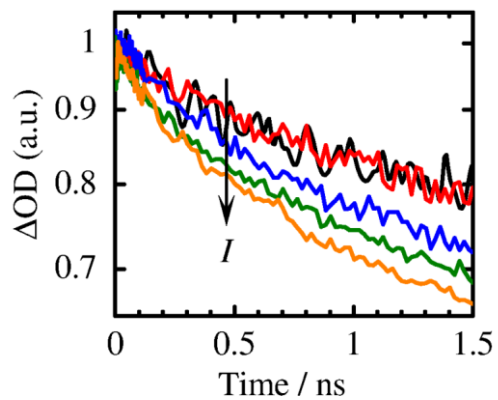


Figure 5. Transient decay at 1240 nm of PCPDTBT polaron in PCPDTBT/PCBM blend film excited at 800 nm with fluences of 1 (black), 20 (red), 30 (blue), 50 (green), and 80 (orange) $\mu\text{J cm}^{-2}$.

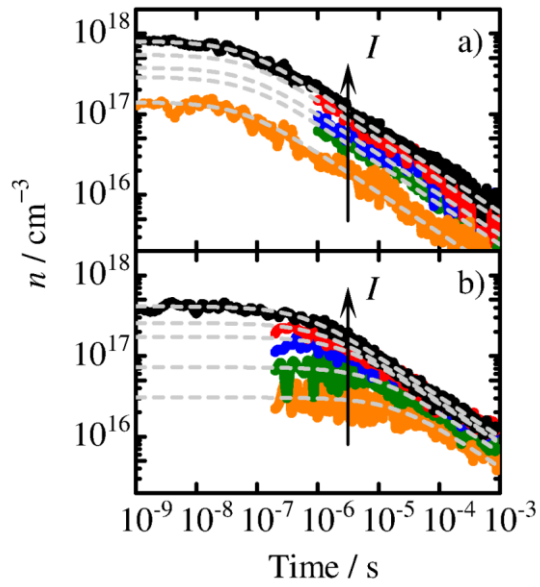


Figure 6. Transient decay of polymer polarons with fluences of 1 (orange), 2 (gray), 5 (green), 10 (red) and 20 $\mu\text{J cm}^{-2}$ (black): a) PCPDTBT polaron (1240 nm) in PCPDTBT/PCBM blends excited at 800 nm and b) P3HT polaron (1000 nm) in RR-P3HT/PCBM blends excited at 400 nm. The gray broken lines show the fitting curves by a power-law function: $n(t) = n_0(1 + at)^{-\alpha}$ with $\alpha = 0.5$.

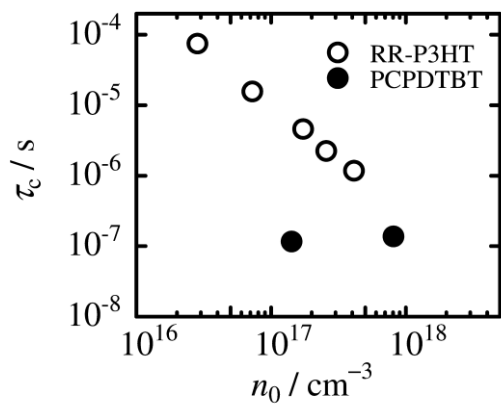
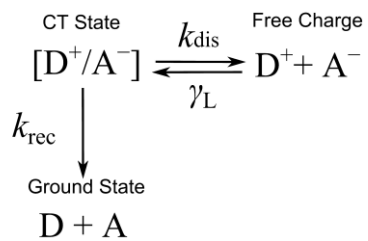


Figure 7. Charge carrier lifetime τ_c defined by Equation 4 plotted against the initial charge carrier density n_0 : PCPDTBT polaron in PCPDTBT/PCBM blends (closed circles) and P3HT polaron in RR-P3HT/PCBM blend films (open circles).

SCEHEME TITLES

Scheme 1. Kinetic scheme for the bimolecular recombination via the interfacial CT state.



γ_L : the Langevin recombination rate, k_{rec} : the geminate recombination rate of the CT state, k_{dis} : the charge dissociation rate into free carriers from the CT state

ASSOCIATED CONTENT

Supporting Information Available: Full description of the material. This material is available free of charge via the Internet at <http://pubs.acs.org>.

AUTHOR INFORMATION

Corresponding Author

*E-mail: ohkita@photo.polym.kyoto-u.ac.jp. Tel.: +81 75 383 2613. Fax: +81 75 383 2617

Author Contributions

The manuscript was written through contributions of all authors. All authors have given approval to the final version of the manuscript.

REFERENCES AND NOTE

- (1) Green, M. A.; Emery, K.; Hishikawa, Y.; Warta, W.; Dunlop, E. D. *Prog. Photovolt. Res. Appl.* **2012**, *20*, 12–20.
- (2) Service, R. F. *Science* **2011**, *332*, 293.
- (3) Mullekom, H. A. M.; Vekemans, J. A. J. M.; Havinga, E. E.; Meijer, E. W. *Mater. Sci. Eng.* **2001**, *32*, 1–40.
- (4) Bundgaard, E.; Krebs, F. C. *Sol. Energy Mater. Sol. Cells* **2007**, *91*, 954–985.
- (5) Ohkita, H.; Ito, S. *Polymer* **2011**, *52*, 4397–4417.
- (6) Mühlbacher, D.; Scharber, M.; Morana, M.; Zhu, Z.; Waller, D.; Gaudiana, R.; Brabec, C. *Adv. Mater.* **2006**, *18*, 2884–2889.
- (7) Peet, J.; Kim, J. Y.; Coates, N. E.; Ma, W. L.; Moses, D.; Heeger, A. J.; Bazan, G. C. *Nat. Mater.* **2007**, *6*, 497–500.
- (8) Moet, D. J. D.; Lenes, M.; Morana, M.; Azimi, H.; Brabec, C. J.; Blom, P. W. M. *Appl. Phys. Lett.* **2010**, *96*, 213506.
- (9) Bijleveld, J. C.; Shahid, M.; Gilot, J.; Wienk, M. M.; Janssen, R. A. J. *Adv. Funct. Mater.* **2009**, *19*, 3262–3276.
- (10) Brenner, T. J. K.; Li, Z.; McNeil, C. R. *J. Phys. Chem. C* **2011**, *115*, 22075–22083.
- (11) Hwang, I. W.; Soci, C.; Moses, D.; Zhu, Z.; Waller, D.; Gaudiana, R.; Brabec, C. J.; Heeger, A. J. *Adv. Mater.* **2007**, *19*, 2307–2312.
- (12) Hwang, I. W.; Cho, S.; Kim, C. J.; Lee, K.; Coates, N. E.; Moses, D.; Heeger, A. J. *J. Appl. Phys.*

2008, 104, 033706.

- (13) Lenes, M.; Morana, M.; Brabec, C. J.; Blom, P. W. M. *Adv. Funct. Mater.* **2009**, *19*, 1106–1111.
- (14) Li, Z.; McNeill, C. R. *J. Appl. Phys.* **2011**, *109*, 074513.
- (15) Maurano, A.; Hamilton, R.; Shuttle, C. G.; Ballantyne, A. M.; Nelson, J.; Zhang, W.; McCulloch, I.; Azimi, H.; Morana, M.; Brabec, C. J.; et al. *Adv. Mater.* **2010**, *22*, 4987–4992.
- (16) Yamamoto, S.; Ohkita, H.; Benten, H.; Ito, S. *Adv. Funct. Mater.* **2012**, DOI: 10.1002/adfm.201200086.
- (17) Agostinelli, T.; Ferenczi, T. A. M.; Pires, E.; Foster, S.; Maurano, A.; Müller, C.; Ballantyne, A.; Hampton, M.; Lilliu, S.; Campoy-Quiles; et al. *J. Polym. Sci. B: Polym. Phys.* **2011**, *49*, 717–724.
- (18) Morana, M.; Azimi, H.; Dennler, G.; Egelhaaf, H.-J.; Scharber, M.; Forberich, K.; Hauch, J.; Gaudiana, R.; Waller, D.; Zhu, Z.; et al. *Adv. Funct. Mater.* **2010**, *20*, 1180–1188.
- (19) Guo, J.; Ohkita, H.; Benten, H.; Ito, S. *J. Am. Chem. Soc.* **2009**, *131*, 16869–16880.
- (20) Clarke, T.; Ballantyne, A.; Jamieson, F.; Brabec, C.; Nelson, J.; Durrant, J. *Chem. Commun.* **2009**, 89–91.
- (21) Jamieson, F. C.; Agostinelli, T.; Azimi, H.; Nelson, J.; Durrant, J. R. *J. Phys. Chem. Lett.* **2010**, *1*, 3306–3310.
- (22) Yamamoto, S.; Guo, J.; Ohkita, H.; Ito, S. *Adv. Funct. Mater.* **2008**, *18*, 2555–2562.
- (23) Grancini, G.; Martino, N.; Antognazza, M. R.; Celebrano, M.; Egelhaaf, H.-J.; Lanzani, G. *J. Phys. Chem. C* **2012**, *116*, 9838–9844.
- (24) Guo, J.; Ohkita, H.; Yokoya, S.; Benten, H.; Ito, S. *J. Am. Chem. Soc.* **2010**, *132*, 9631–9637.

- (25) Nelson, J. *Phys. Rev. B* **2003**, *67*, 155209.
- (26) Guo, J.; Ohkita, H.; Bente, H.; Ito, S. *J. Am. Chem. Soc.* **2010**, *132*, 6154–6164.
- (27) Lee, J. K.; Ma, W. L.; Brabec, C. J.; Yuen, J.; Moon, J. S.; Kim, J. Y.; Lee, K.; Bazan, G. C.; Heeger, A. J. *J. Am. Chem. Soc.* **2008**, *130*, 3619–3623.
- (28) Albrecht, S.; Schindler, W.; Kurpiers, J. *J. Phys. Chem. Lett.* **2012**, *3*, 640–645.
- (29) Gu, Y.; Wang, C.; Russell, T. P. *Adv. Energy Mater.* **2012**, *2*, 683–690.
- (30) Etzold, F.; Howard, I. A.; Mauer, R.; Meister, M.; Kim, T. D.; Lee, K. S.; Beak, N. S.; Laquai, F. *J. Am. Chem. Soc.* **2011**, *133*, 9469–9479.
- (31) Chen, H. Y.; Hou, J.; Hayden, A. M.; Yang, H.; Houk, K. N.; Yang, Y. *Adv. Mater.* **2009**, *21*, 371–375.
- (32) Rogers, J. T.; Schmidt, K.; Toney, M. F.; Kramer, E. J.; Bazan, G. C. *Adv. Mater.* **2011**, *23*, 2284–2288.
- (33) Jarzab, D.; Cordella, F.; Gao, J.; Scharber, M.; Egelhaaf, H.-J.; Loi, M. A. *Adv. Energy Mater.* **2011**, *1*, 604–609.
- (34) Etzold, F.; Howard, I. A.; Forler, N.; Cho, D. M.; Meister, M.; Mangold, H.; Shu, J.; Hansen, M. R.; Müllen, K.; Laquai, F. *J. Am. Chem. Soc.* **2012**, DOI: 10.1021/ja303154g.
- (35) The interaction radius was estimated from the absorbance immediately after the laser excitation (<0.1 ps). Here we ascribe the long-range interaction of singlet excitons at <0.1 ps to the exciton delocalization as reported previously, because the dipole–dipole interaction of singlet excitons and the exciton migration are negligible on such a short timescale (<0.1 ps). Note that the delocalization of polymer singlet excitons in blends is almost the same as in a neat film because no change in the

absorption band of polymer singlet excitons is observed.

- (36) Dogariu, A.; Vacar, D.; Heeger, A. J. *Phys. Rev. B* **1998**, *58*, 10218–10224.
- (37) Clarke, T. M.; Durrant, J. R. *Chem. Rev.* **2010**, *110*, 6736–6767.
- (38) Schwarz, C.; Bäessler, H.; Bauer, I.; Koenen, J. M.; Preis, E.; Scherf, U.; Köhler, A. *Adv. Mater.* **2012**, *24*, 922–925.
- (39) Pivrikas, A.; Juška, G.; Mozer, A. J.; Scharber, M.; Arlauskas, K.; Sariciftci, N. S.; Stubb, H.; Österbacka, R. *Phys. Rev. Lett.* **2005**, *94*, 176806.
- (40) Baumann, A.; Lorrmann, J.; Deibel, C.; Dyakonov, V. *Appl. Phys. Lett.* **2008**, *93*, 252104.
- (41) Hilczer, M.; Tachiya, M. *J. Phys. Chem. C* **2010**, *114*, 6808–6813.
- (42) Ferguson, A. J.; Kopidakis, N.; Shaheen, S. E.; Rumbles, G. *J. Phys. Chem. C* **2011**, *115*, 23134–23148.
- (43) Yamamoto, S.; Orimo, A.; Ohkita, H.; Benten, H.; Ito, S. *Adv. Energy Mater.* **2012**, *2*, 229–237.
- (44) Pope, M.; Swenberg, C. E. *Electronic Processes in Organic Crystals and Polymers, Second Edition*; Oxford University Press: New York, **1999**.
- (45) Howard, I. A.; Mauer, R.; Meister, M.; Laquai, F. *J. Am. Chem. Soc.* **2010**, *132*, 14866–14876.
- (46) Marsh, R. A.; Hodgkiss, J. M.; Albert-Seifried, S.; Friend, R. H. *Nano Lett.* **2010**, *10*, 923–930.

SYNOPSIS

